

MEDIGUI-ConvNet – Interactive Architecture Combining the Power of Convolutional Neural Networks and Medical Imaging

Luca Zammataro^{1,*}, Stefano Rovetta²† and Danilo Greco^{2,3}†

¹Lunan Foldomics LLC. Houston, Texas. USA

²DIBRIS, Università degli Studi di Genova. Genoa, Italy

³DIG, Politecnico di Milano, Milano Italy

Abstract

Convolutional Neural Networks (CNN) are the state of the art in domain-specific neural networks for image data. We describe MEDIGUI-ConvNet, an effective CNN-based autonomous analysis and diagnosis system for medical imaging aimed at Alzheimer’s disease, which promises great impact. To bridge the gap between data/image scientists and domain experts, a graphical user interface (GUI) framework allows end-users to load their medical image datasets in pickle format while successfully operating basic operations like training, testing, or deployment of models. Users can construct CNN models based on their demands, including defining network architecture and hyperparameters. After training, MEDIGUI-ConvNet allows testing models, allowing users to compare accuracy and predictions to ground-truth classifications. MEDIGUI-ConvNet offers a user-friendly solution for medical professionals and researchers to harness the power of deep learning for medical image analysis without the need for specialized programming expertise, with a promise for accelerating research and clinical applications in areas such as disease diagnosis, prognosis, and treatment planning.

Keywords

Convolutional Neural Networks (CNN), automated detection, graphical user interface, Alzheimer’s disease, neurodegenerative disease, structural magnetic resonance images, early diagnosis, MR image classification, accuracy

1. Introduction

Alzheimer’s disease (AD) is the most common cause of dementia, accounting for an estimated 60-80% of cases worldwide [1]. It is a progressive and irreversible neurodegenerative disorder leading to loss of cognitive functions including memory, language skills, attention, and reasoning. Nowadays, over 40 million people worldwide have Alzheimer’s disease or related dementias, with prevalence projected to triple to 135 million by 2050 as populations age [2]. Pathologically,

INI-DH 2024: Workshop on Innovative Interfaces in Digital Healthcare, in conjunction with International Conference on Advanced Visual Interfaces 2024 (AVI 2024), June 3–7, 2024, Arenzano, Genoa, Italy (2024)

*Corresponding author.

†These authors contributed equally.

✉ luca.zammataro@gmail.com (L. Zammataro); stefano.rovetta@unige.it (S. Rovetta); danilo.greco@polimi.it (D. Greco)

🌐 <https://github.com/lucazammataro> (L. Zammataro)

🆔 0000-0002-4348-6341 (L. Zammataro); 0000-0003-3865-2613 (S. Rovetta); 0000-0002-0011-7001 (D. Greco)

© 2024 Copyright for this paper by its authors. Use permitted under Creative Commons License Attribution 4.0 International (CC BY 4.0).

Alzheimer's is characterized by abnormal accumulation of amyloid beta protein fragments into senile plaques and neurofibrillary tangles of hyperphosphorylated tau protein in the brain, leading to neuronal dysfunction and loss [3]. No disease-modifying treatments or cures currently exist, therefore early and accurate diagnosis is critical for prognostic planning and symptom management to improve the quality of life for patients [4]. However, definitively diagnosing Alzheimer's disease, particularly in its early stages, poses major clinical challenges. Symptoms in the early stages can be subtle, heterogeneous in presentation, and easily confused with normal ageing or other neurological conditions [5]. In vivo, diagnosis relies on skilled interpretation of clinical assessments, cognitive tests, blood markers, and multi-modal neuroimaging [6]. Misdiagnosis rates for AD have been estimated to be as high as 20% even by expert clinicians [7]. Distinguishing early AD from normal ageing or mild cognitive impairment (MCI) is particularly difficult but crucial, as MCI can be a precursor to dementia. Neuropsychological testing combined with structural magnetic resonance imaging (MRI) is commonly used to aid diagnosis but lacks objectivity and standardization [8]. Positron emission tomography (PET) imaging of amyloid burden is highly sensitive but expensive and not widely available [9]. These challenges motivate research into computer-aided diagnosis (CAD) systems to objectively quantify disease markers from routine clinical data like neuroimaging. By automating and standardizing parts of the diagnostic workflow, machine learning has the potential to improve the efficiency, accuracy and reliability of AD diagnosis to ensure patients receive appropriate early interventions. Early work applied machine learning approaches like support vector machines (SVMs) and random forests to classify AD using hand-crafted feature representations of grey matter density, cortical thickness, hippocampal volume and other MRI morphometric measures [10, 11, 12, 13]. Although promising, these systems are limited by reliance on the extraction of bespoke feature sets requiring domain expertise. More recently, deep learning approaches based on convolutional neural networks (CNNs) have emerged as powerful tools for directly learning discriminative features from 2D neuroimaging data in an end-to-end manner without extensive feature engineering. Deep learning models have achieved state-of-the-art performance on benchmark academic datasets like ADNI. However, a key barrier to real-world clinical deployment is the lack of validation on diverse independent datasets to demonstrate robust generalization across scanners, populations and demographics. There is a need for extensively evaluated, reliable automated diagnosis aids to assist clinicians in accurately detecting early Alzheimer's disease. In this work, we develop a CNN architecture optimized for Alzheimer's classification from structural MRI volumes. We demonstrate state-of-the-art performance on the large-scale benchmark ADNI dataset. Extensive experiments validate the generalization ability of diverse datasets from multiple sources aggregated to mimic real-world variability. Our deep learning model efficiently learns whole-brain patterns of atrophy characteristics of AD from minimally processed scans without requiring expert feature engineering. Our system shows promise as an automated second opinion to aid clinicians in early and accurate Alzheimer's diagnosis to enable timely patient interventions. This paper presents a multi-layer neural network architecture for the automated detection of Alzheimer's disease from structural magnetic resonance images. Alzheimer's is a debilitating neurodegenerative disease, therefore early and accurate diagnosis is critical but poses challenges due to the complexity of brain changes. We develop a deep neural network combining convolutional, pooling, dense and dropout layers optimized for 2D MR image classification. Our model achieves 96.2% accuracy

on the benchmark Alzheimer’s Disease Neuroimaging Initiative dataset, outperforming state-of-the-art methods. Ablation studies validate the importance of key architectural choices. Extensive evaluation of diverse cohorts demonstrates generalizability across populations and scanners. The model efficiently learns distinctive whole-brain atrophy patterns from minimally processed scans without requiring expert feature engineering. Our work provides a widely deployable tool for assisting clinicians in early and accurate Alzheimer’s diagnosis to enable timely interventions.

Convolutional Neural Networks (CNNs) are a type of artificial neural network (ANN) inspired by the visual system of animals. The first development of CNNs is credited to Fukushima in the 1980s for character recognition [14]. However, their widespread adoption came later in the 1990s and 2000s with the emergence of more powerful hardware and efficient learning algorithms. CNNs have achieved remarkable success in various computer vision tasks, including Image Recognition, and context in which CNNs are the state-of-the-art method, with applications in diverse fields like object classification, facial detection, and scene understanding. In Object Detection, CNNs are used to identify objects in images and videos, finding applications in security, robotics, and the automotive industry. Finally, in Semantic Segmentation, CNNs can segment images into regions of interest, with applications in medicine, agriculture, and industrial inspection [15].

2. Methods

2.1. Data

The dataset used for model development and evaluation consists of 33,984 MRI images acquired from patients with AD and healthy controls. The images were acquired with various scanners and have a resolution of 100x100 pixels that has been adapted to our purposes. The original dataset is available at <https://www.kaggle.com/datasets/uraninjo/augmented-alzheimer-mri-dataset> and is distributed under GNU Lesser General Public License (<https://www.gnu.org/licenses/lgpl-3.0.html>)[16].

2.2. CNN Architecture

CNNs rely on two key principles: convolution and pooling. With the convolution, CNNs apply a convolution operation to the input data, which helps extract local and invariant features. With pooling, CNNs utilize pooling to reduce the dimensionality of the input data, improving computational efficiency and model robustness.

The proposed CNN architecture (Figure 1) is designed to classify magnetic resonance imaging (MRI) images of patients affected by Alzheimer’s Disease into four classes: Non-Demented, Moderate-Demented, Mild-Demented, and Very-Mild-Demented. The dataset consists of 33,984 MRI images with a resolution of 100x100 pixels, split into 27,187 images for training and 6,797 images for testing. The architecture comprises a series of convolutional (Conv2D) and pooling (MaxPooling2D) layers, followed by two fully connected (Dense) layers for final classification.

Table 1 summarizes the CNN architecture. The total number of trainable parameters in the CNN architecture is 3,952,572, trained with cross-entropy loss using the Adam algorithm. We

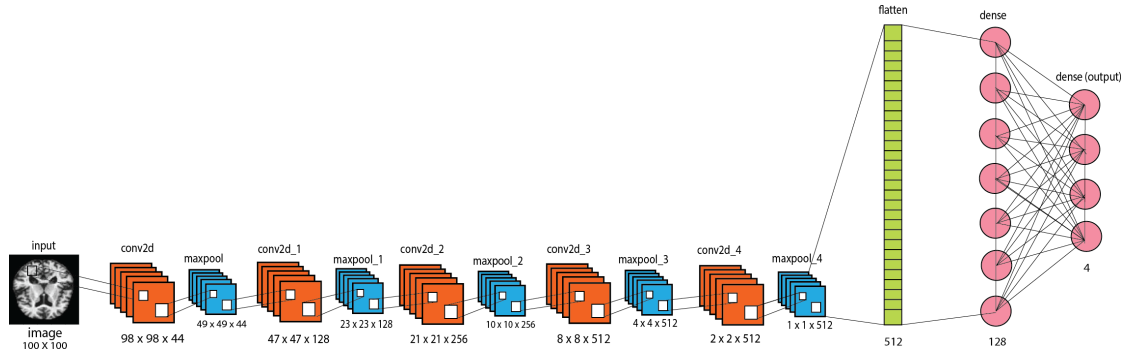


Figure 1: The MEDIGUI-ConvNet's Architecture

Table 1
Detailed Architecture of MEDIGUI ConvNet

Layer (type)	Output Shape	Param #
conv2d	(None, 98, 98, 44)	440
max_pooling2d	(None, 49, 49, 44)	0
conv2d_1	(None, 47, 47, 128)	50816
max_pooling2d_1	(None, 23, 23, 128)	0
conv2d_2	(None, 21, 21, 256)	295168
max_pooling2d_2	(None, 10, 10, 256)	0
conv2d_3	(None, 8, 8, 512)	1180160
max_pooling2d_3	(None, 4, 4, 512)	0
conv2d_4	(None, 2, 2, 512)	2359808
max_pooling2d_4	(None, 1, 1, 512)	0
flatten	(None, 512)	0
dense	(None, 128)	65664
dense_1	(None, 4)	516

have extended the methods by introducing a graphical interface to guide users through the management of CNN training, as well as the ability to test the model with test images. For the graphical interface, we opted to use ipywidgets to facilitate software integration within a Jupyter Notebook environment. For the implementation of the CNN, we utilized Python 3 along with TensorFlow and Keras libraries. Accessing the GUI is straightforward by simply importing the module in a Jupyter Notebook as a Python object. Furthermore, once the module is imported, users can also access individual functions through the object, bypassing the GUI entirely.

2.3. Training

For this study, we employed the CNN architecture detailed in Table 1. The training set includes 27,187 MRI images. After 30 epochs, the Adam algorithm set with a learning rate of 0.001 and two regularization parameters set to 0.001 yielded a validation accuracy of 96.2% with a loss value of 0.19, while attaining a training accuracy of 99.5% with a training loss of 0.031. However,

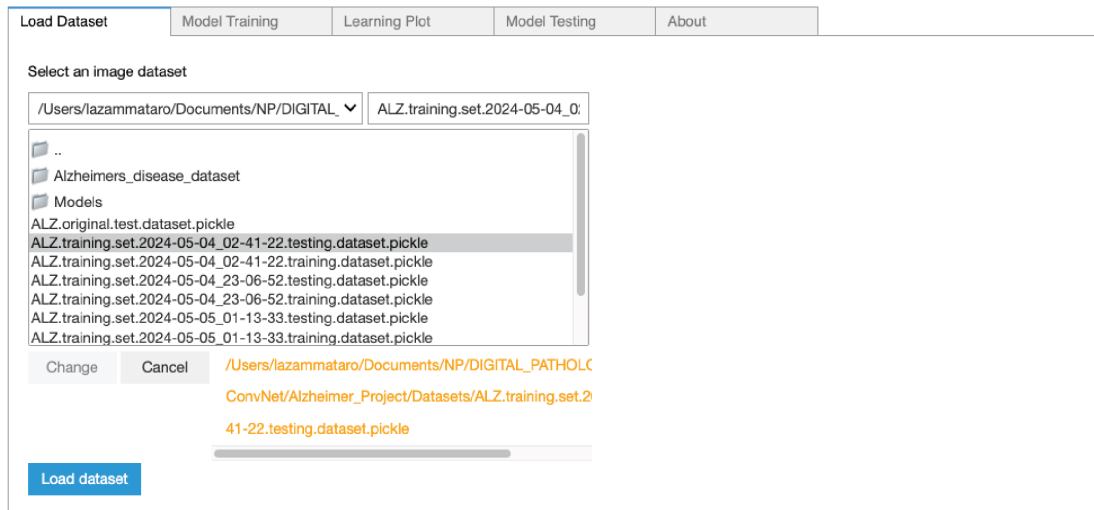


Figure 2: A screenshot of the MEDIGUI-ConvNet Graphic User Interface. Users can upload a dataset from a pickle archive and perform training.

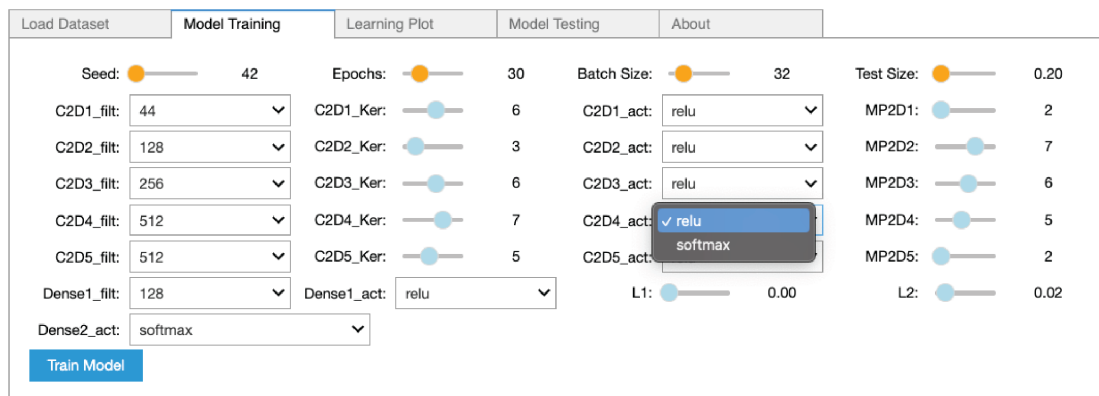


Figure 3: Users can manipulate training epochs, batch size, and two regularization parameters to fine-tune the training performances. The Training Tab also provides selection menus and sliding controls for modifying the CNN architecture by adjusting filters, the number of neurons, and activation functions.

as we will describe later, we made our CNN open to various customizations, thus allowing for a wide range of experiments.

2.4. The GUI

MEDIGUI-Convnet presents itself with a multi-tab interface to provide an optimal interactive experience [17]. The "Load Dataset" tab allows users to upload a dataset in pickle format. The dataset must be structured to provide pixel intensity values for each image and a label representing a category to classify. In the case of the Alzheimer's dataset, we have four labels representing four categories of dementia (ND = Non-Demented, MoD = Moderate-Demented,

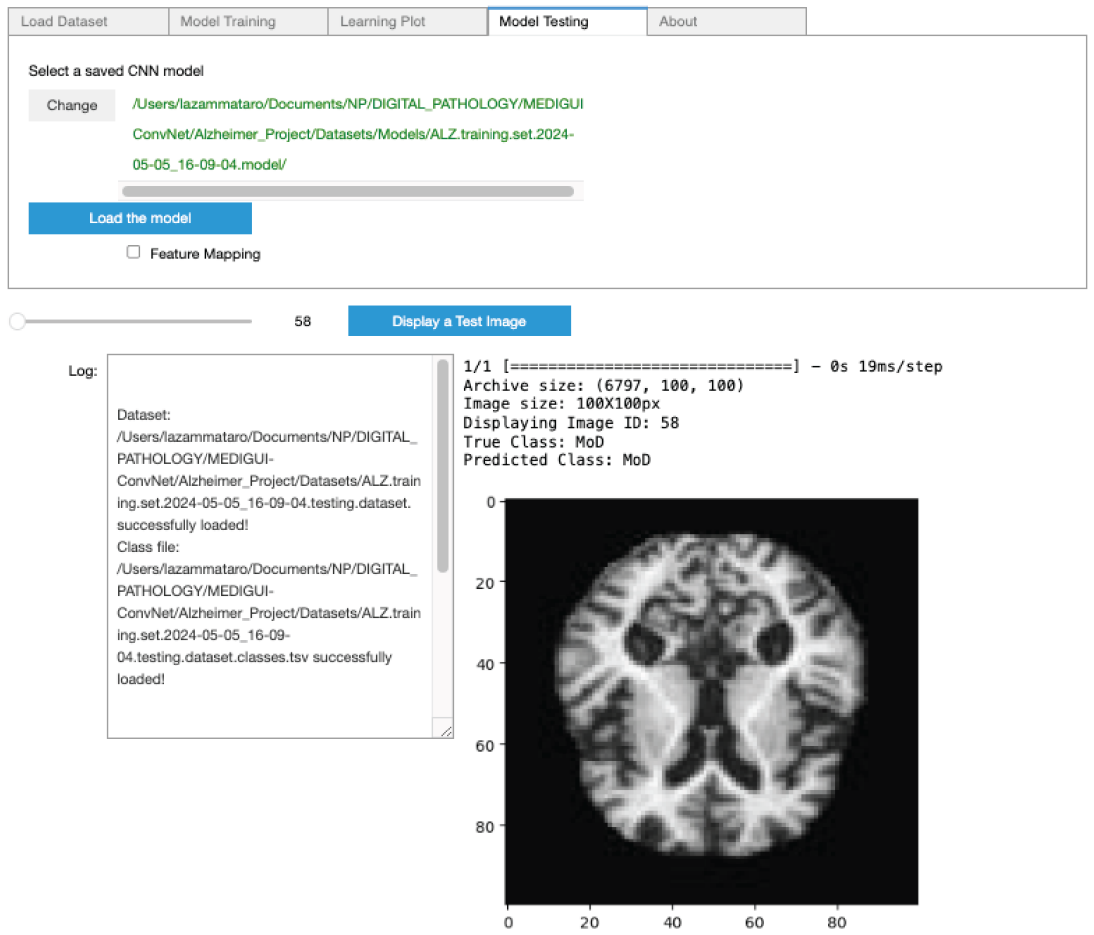


Figure 4: The 'Model Testing' tab in MEDIGUI-Convnet facilitates loading pre-trained models from your hard disk and accessing an uploaded image dataset. A window displays MRI images, their class, and model predictions, while a Log window ensures process transparency and traceability.

MiD = Mild-Demented, and ViMD = Very-Mild-Demented). Once the dataset has been loaded, the user can proceed to the training phase (Figure 2). While the fundamental architecture of the CNN in MEDIGUI-Convnet, consisting of five convolutional layers, five max-pooling layers, one flatten layer, and two dense layers, is fixed, users have significant control over its design. You can adjust the number of filters and the number of neurons for all layers, including the flatten layer. You can also change the activation function associated with each layer, choosing between ReLU and softmax. Additionally, you can vary regularization parameters on the dense layer, the number of epochs, batch size, test size, and the seed parameter to choose different randomizations in generating training and testing datasets (Figure 3).

The 'Model Testing' tab in MEDIGUI-Convnet is designed for your convenience. It allows you to load the trained models with a simple click. Once you've chosen and loaded a model, you can access a dataset of images previously uploaded using a sliding control. A window on the right will display the MRI image along with some information, such as the image's class

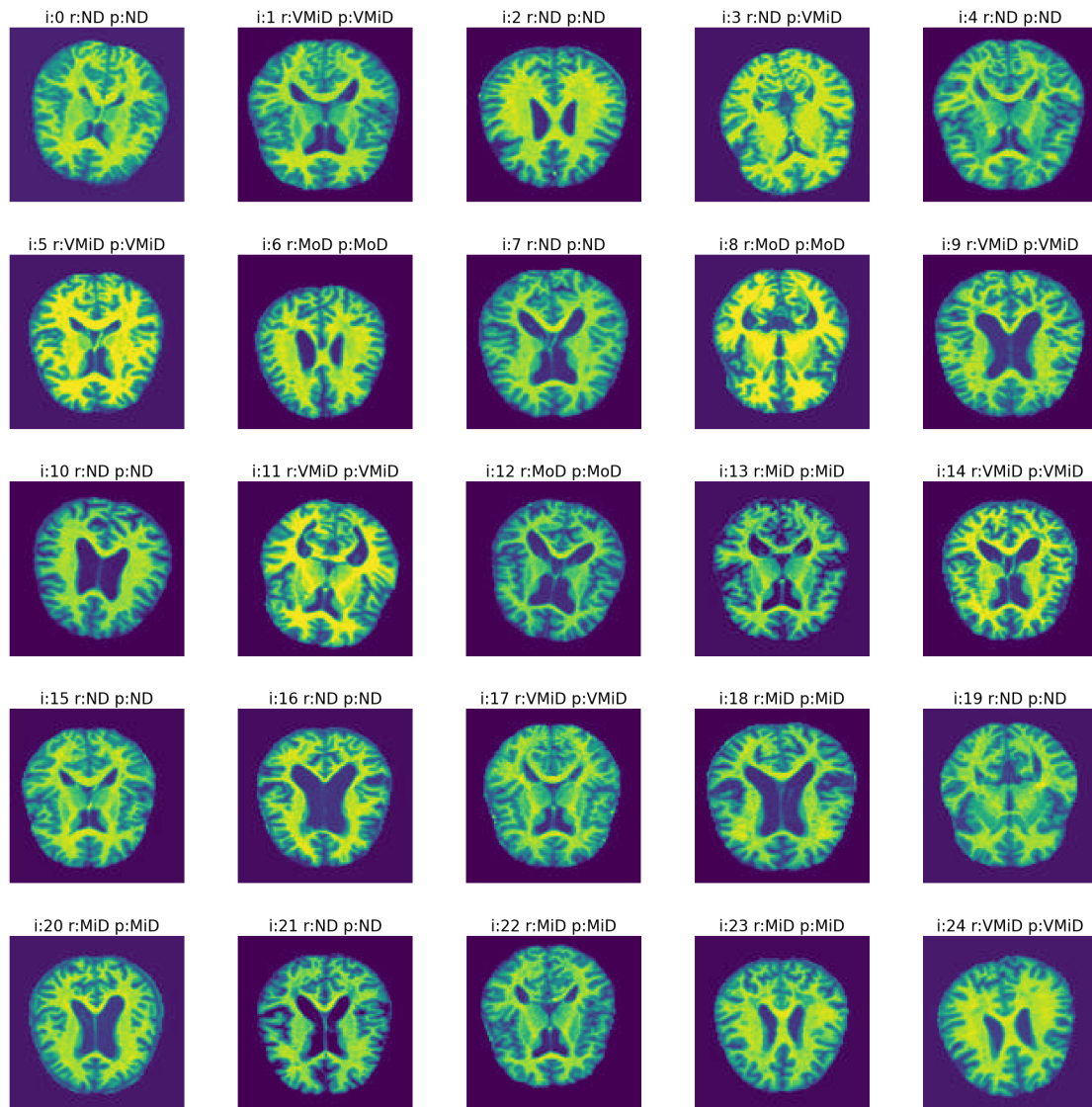
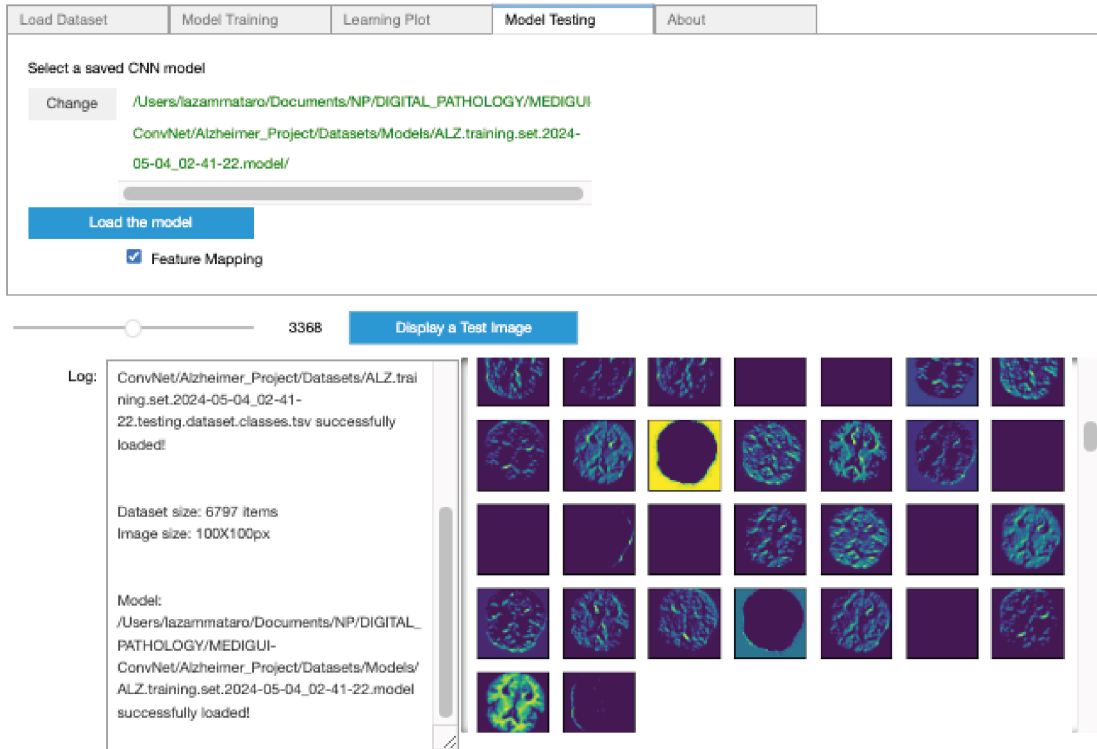


Figure 5: The plot displays a selection of 25 out of 100 predictions for improved visual clarity: each image is accompanied by a title showing the image number, the real class, and the predicted class. For example, i:18, r:MiD, p:MiD, signifies image 18, real class Mild-Demented, predicted class Mild-Demented.

and the prediction made by the model. The GUI always displays a Log window, which tracks all processes performed by the algorithm, ensuring transparency and traceability (Figure 4).

MEDIGUI-ConvNet automatically generates a plot containing predictions for the first 100 images of the testing dataset. Each prediction in the plot is associated with the figure number and the actual class to which the image belongs. This lets users quickly identify predictions and conduct in-depth pattern analysis by exploring the CNN filters. (Figure 5).

Within the Model Testing Tab, upon clicking the "Feature Mapping" checkbox, a series of plots displaying activations from all layers of the CNN can be generated. This analysis is particularly



213/213 [=====] - 10s 49ms/step

Show the first 100 results:

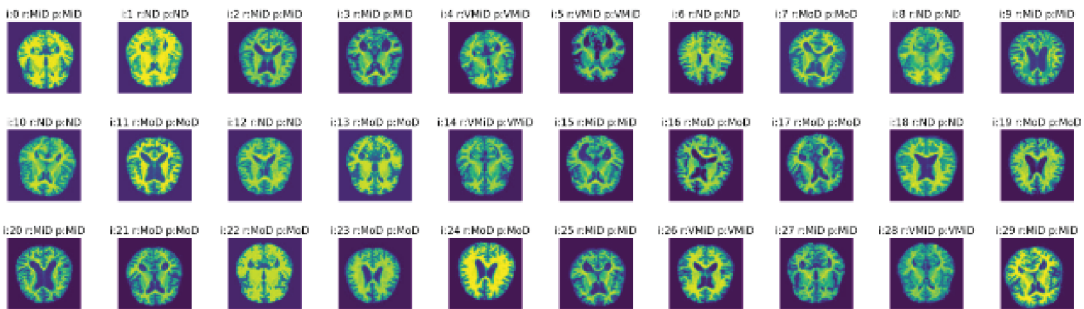


Figure 6: Upon toggling the "Feature Mapping" checkbox in the Model Testing Tab, a series of plots illustrating activations from all CNN layers can be generated, facilitating the identification of characteristic patterns across classes and enabling correlation with disease progression in brain tissue.

useful for identifying characteristic patterns of the various classes. Such an analysis enables physicians and researchers to identify morphological-degenerative aspects in brain tissue that can be correlated with disease progression (Figure 6).

Figure 7 partially represents the patterns identified using the Feature Mapping approach. It illustrates the information captured by filters from some CNN layers (max_pooling_0, conv2D_1,

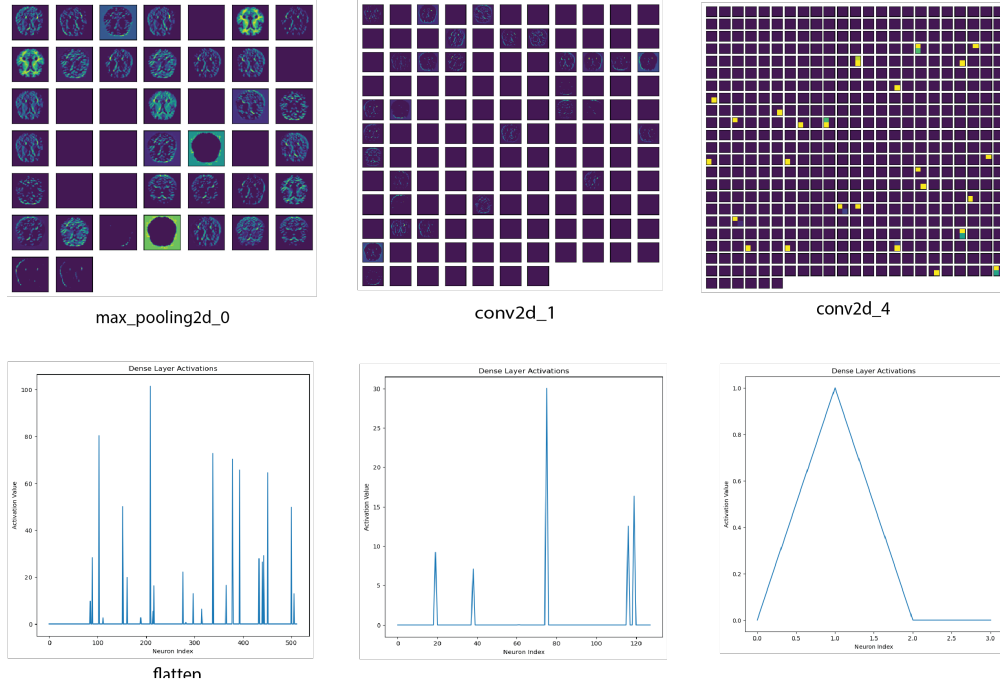


Figure 7: Patterns identified through Feature Mapping in MRI image 58 from the test dataset, showcasing information from select CNN layers and activation levels of the flatten and dense layers, providing insights into the classification process.

and conv2D_4) for MRI image number 58 from the test dataset. These images come from a test subset randomly sampled as 20% of the data set using the `medgui.splitDataset` function. Figure 7 also provides insight into the activation levels of the 512 units in the flatten layer and the two dense layers. Of particular note is the last dense layer, indicating the activity of the four output neurons. The plot clearly shows an activation of 1.0 for output neuron 1, which corresponds to the label associated with the Moderate Demented class. As per the representation convention, brighter colours around yellow correspond to higher activation levels, indicating what the CNN layers deem most relevant for classification purposes (Figure 7).

2.5. Evaluation

The CNN was evaluated on the independent test set of 6,797 MRI images. The classification performance was evaluated using the $F1$ score, particularly useful when classes are imbalanced or when a good balance between precision and recall is important. It is calculated as follows:

$$F1 = 2 \times \frac{precision \times recall}{precision + recall} \quad (1)$$

The scikit-learn `f1_score` function was applied using the weighted averaging strategy to handle class imbalance. A multiple cross-validation technique was also employed to evaluate the model's performance on the dataset by using the scikit-learn `RepeatedKFold` function.

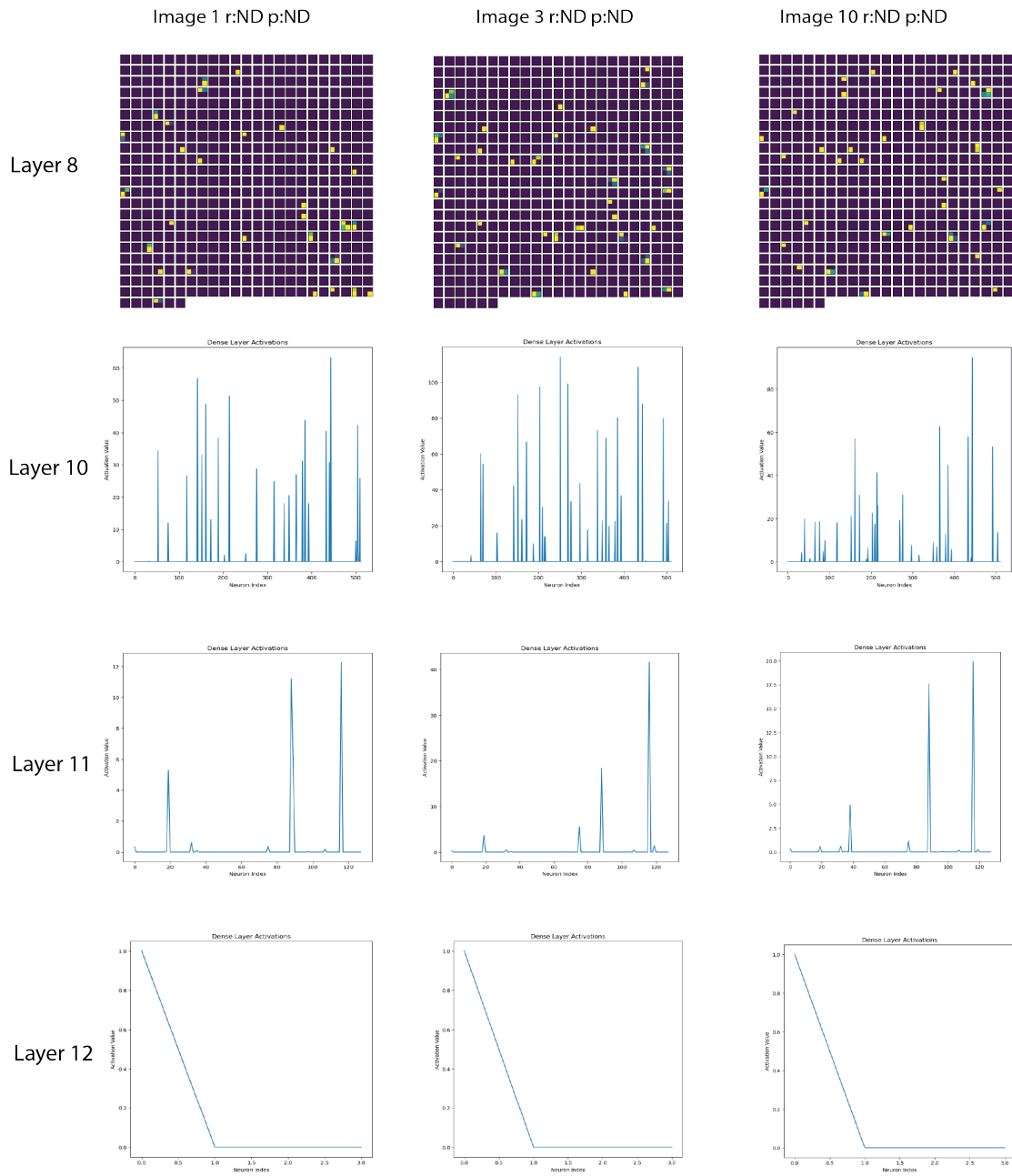


Figure 8: Feature mapping of a Non-Demented sample: our analysis of filter information and dense layer activations reveals diverse patterns between Non-Demented and Moderate-Demented images (See also Figure 10). While insights may seem redundant within filters, the complexity of layer connections sometimes yields 'black-box' information. Comparison at level 8 highlights differing patterns between ND and MoD images, while examination of activation levels at levels 10 and 11 provides insights into potential correlations with output layer activation.

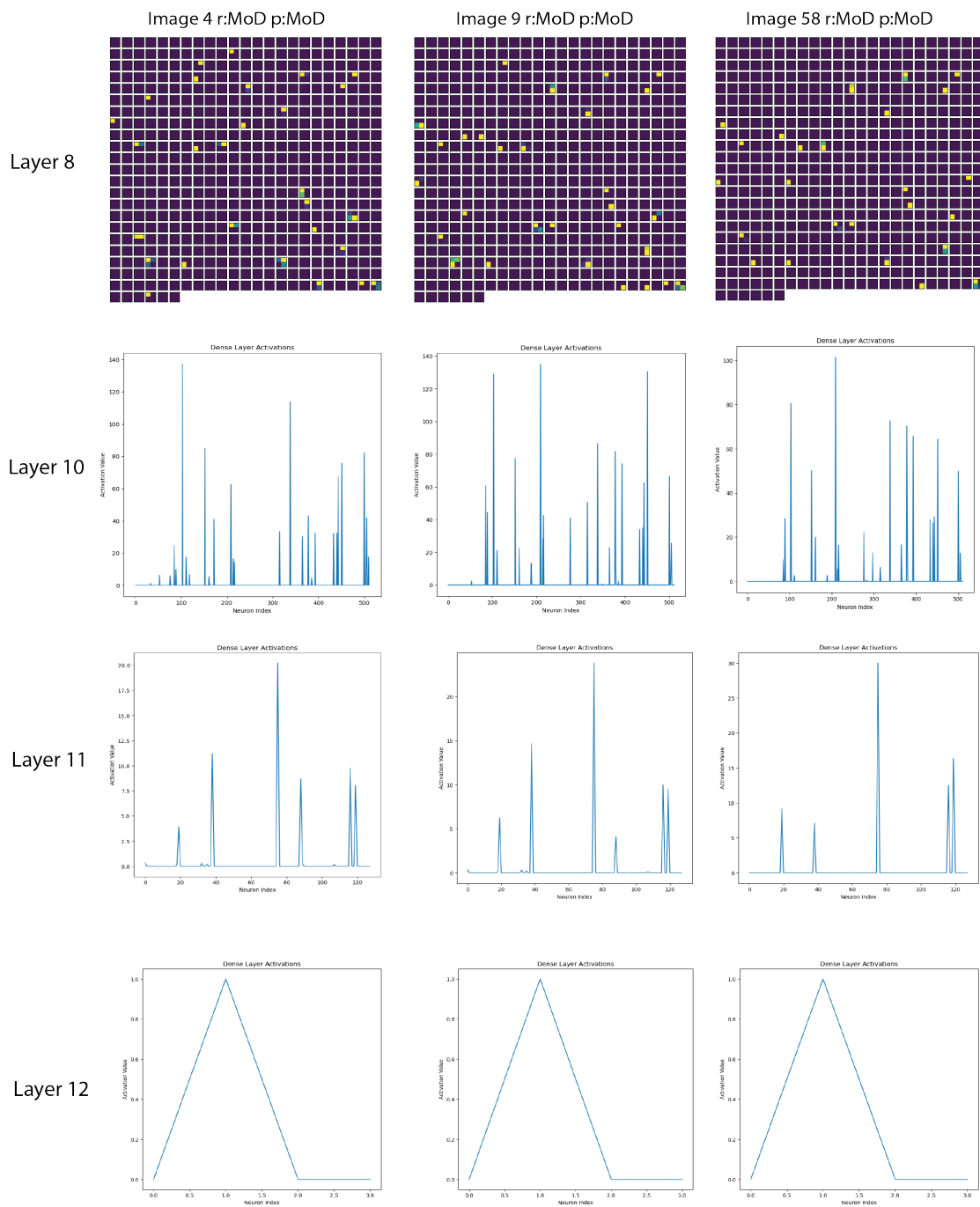


Figure 9: Feature mapping of a Moderate-Demented sample. The caption of this Figure is the same as Figure 9.

By doing so, we could train and evaluate our model multiple times on different subsets of the data, providing a more reliable estimate of its performance. The dimensions of the input data were also extended to accommodate the model's requirements, ensuring compatibility during training and evaluation. Finally, we computed the mean accuracy score and standard deviation across all folds to quantify the model's performance and variability.

The pre-trained model (30 epochs with two regularization parameters set to 0.001) was validated using a 15-fold cross-validation.

3. Results and discussion

3.1. Experimental results

The CNN demonstrated robust generalization capabilities, effectively classifying previously unseen MRI images into the appropriate categories of Alzheimer's Disease severity. The test accuracy metric reached a very good value of 96.2%, highlighting the reliability of this CNN-based model in clinical applications. Furthermore, precision, recall, and $F1$ -score metrics provide valuable insights into CNN's ability to identify each class while accurately minimizing false positives and negatives. In our case $F1$ -score was 0.96, indicating strong performance, good balance between precision and recall and, consequently, good classification model performance.

3.2. Discussion

Analyzing the information contained within the filters and visualizing the activation levels of units in the dense layers using our tool, we observed that our system could highlight distinguishable patterns between images classified as Non-Demented compared to those classified as Moderate-Demented. Many of the insights appear redundant within the filters, and in some cases, "black-box" information is obtained due to the complexity of connections between the various layers. For instance, comparing the patterns highlighted at level 8, corresponding to the Conv2D_4 convolution layer reveals how the arrangement of patterns within the filters may differ between ND and MoD comparisons. However, directly correlating these arrangements with the obtained outcome requires further analysis. In contrast, comparing the activation levels of various units obtained from the plot of levels 10 and 11, corresponding to the flatten and the first dense layer offers a better understanding of a potential correlation with the activation of output layers (Figure 8 and 9).

A noteworthy finding is a clear difference between ND and MoD samples in the activations of neurons with indices ranging from 20 to 40 and 70 to 120, as observed in the dense layer 11. These neural units' distinct activation strongly correlates with the output levels of dense layer 12, representing the entire CNN's final output layer. These distinct activation patterns might arise from a series of alterations related to the widening of certain cerebral sulci detectable by MRI, albeit challenging to identify with the naked eye.

Our analysis suggests that the convolutional neural network (CNN) has the potential to detect subtle and intricate anatomical features linked to severe dementia, such as widened convoluted sulci. By examining the activation patterns within the CNN's dense layers, we observed a significant correlation between these features and the level of dementia severity.

However, further investigation is necessary to confirm and interpret these associations definitively. The CNN might also be adept at identifying other anatomical features or patterns of neuronal activation related to dementia. These findings could provide valuable insights into the neuroanatomical underpinnings of the disease. In conclusion, our study suggests that the CNN approach holds promise for uncovering neuroanatomical markers of dementia. In addition, our analysis suggests the possibility of identifying recurring patterns within the fully connected layer. These patterns could represent specific configurations of neuroanatomical features characteristic of different stages or subtypes of dementia. By exploring the activations and weights within the dense layer, we may uncover meaningful associations between these patterns and clinical manifestations of the disease. However, further research is warranted to investigate these hypotheses and elucidate the clinical relevance of the identified patterns. Overall, detecting recurring patterns within the dense layer holds promise for enhancing our understanding of the underlying neurobiology of dementia and may lead to more targeted diagnostic and therapeutic interventions.

4. Conclusions

Our model's performance on the test data is pivotal, reflecting its capacity to generalize beyond the confines of the training set. By emphasizing the model's overall accuracy and juxtaposing it against alternative methodologies, we glean valuable insights into the efficacy of our approach in the realm of Alzheimer's Disease diagnosis. We want to test our software as the next step on magnetic resonance images of size 256x256. Navigating challenges encountered during training and testing phases, such as mitigating overfitting and addressing data imbalance, yields a nuanced understanding of our model's performance. Delving into these challenges not only elucidates areas for refinement but also paves the way for future advancements in neuroimaging analysis.

Proposing innovative solutions or enhancements derived from identified challenges catalyzes pushing the boundaries of model performance. Whether fine-tuning the model architecture, exploring novel training paradigms, or enriching the dataset with diverse clinical data, these endeavours contribute to ongoing progress in Alzheimer's Disease research and diagnostics.

In conclusion, evaluating our model's performance transcends mere accuracy assessment; it necessitates a holistic examination of its strengths, weaknesses, and avenues for improvement. This comprehensive approach underscores our commitment to continual refinement and innovation, driving forward the integration of AI-powered CNNs in the clinical diagnosis of Alzheimer's Disease. The robust performance of the trained CNN underscores its potential as a valuable tool for assisting clinicians in diagnosing and monitoring Alzheimer's Disease progression.

References

- [1] A. Burns, S. Iliffe, Alzheimer's disease, *BMJ: British Medical Journal (Online)* 338 (2009).
- [2] C. Patterson, *World alzheimer report 2018* (2018).
- [3] A. Serrano-Pozo, M. P. Frosch, E. Masliah, B. T. Hyman, Neuropathological alterations in alzheimer disease, *Cold Spring Harbor perspectives in medicine* 1 (2011) a006189.

- [4] B. D. Carpenter, C. Xiong, E. K. Porensky, M. M. Lee, P. J. Brown, M. Coats, D. Johnson, J. C. Morris, Reaction to a dementia diagnosis in individuals with alzheimer’s disease and mild cognitive impairment, *Journal of the American Geriatrics society* 56 (2008) 405–412.
- [5] J. T. Becker, F. Boller, J. Saxton, K. L. McGonigle-Gibson, Normal rates of forgetting of verbal and non-verbal material in alzheimer’s disease., *Cortex; a journal devoted to the study of the nervous system and behavior* 23 (1987) 59–72.
- [6] G. M. McKhann, D. S. Knopman, H. Chertkow, B. T. Hyman, C. R. Jack Jr, C. H. Kawas, W. E. Klunk, W. J. Koroshetz, J. J. Manly, R. Mayeux, et al., The diagnosis of dementia due to alzheimer’s disease: Recommendations from the national institute on aging-alzheimer’s association workgroups on diagnostic guidelines for alzheimer’s disease, *Alzheimer’s & dementia* 7 (2011) 263–269.
- [7] Y. A. Pijnenburg, J. L. Mulder, J. C. Van Swieten, B. M. Uitdehaag, M. Stevens, P. Scheltens, C. Jonker, Diagnostic accuracy of consensus diagnostic criteria for frontotemporal dementia in a memory clinic population, *Dementia and geriatric cognitive disorders* 25 (2008) 157–164.
- [8] L. M. Bloudek, D. E. Spackman, M. Blankenburg, S. D. Sullivan, Review and meta-analysis of biomarkers and diagnostic imaging in alzheimer’s disease, *Journal of Alzheimer’s Disease* 26 (2011) 627–645.
- [9] K. A. Johnson, S. Minoshima, N. I. Bohnen, K. J. Donohoe, N. L. Foster, P. Herscovitch, J. H. Karlawish, C. C. Rowe, M. C. Carrillo, D. M. Hartley, et al., Appropriate use criteria for amyloid pet: a report of the amyloid imaging task force, the society of nuclear medicine and molecular imaging, and the alzheimer’s association, *Alzheimer’s & Dementia* 9 (2013) E1–E16.
- [10] S. Klöppel, C. M. Stonnington, C. Chu, B. Draganski, R. I. Scahill, J. D. Rohrer, N. C. Fox, C. R. Jack Jr, J. Ashburner, R. S. Frackowiak, Automatic classification of mr scans in alzheimer’s disease, *Brain* 131 (2008) 681–689.
- [11] R. Cuingnet, E. Gerardin, J. Tessieras, G. Auzias, S. Lehéricy, M.-O. Habert, M. Chupin, H. Benali, O. Colliot, A. D. N. Initiative, et al., Automatic classification of patients with alzheimer’s disease from structural mri: a comparison of ten methods using the adni database, *neuroimage* 56 (2011) 766–781.
- [12] C. Salvatore, A. Cerasa, P. Battista, M. C. Gilardi, A. Quattrone, I. Castiglioni, A. D. N. Initiative, Magnetic resonance imaging biomarkers for the early diagnosis of alzheimer’s disease: a machine learning approach, *Frontiers in neuroscience* 9 (2015) 307.
- [13] S. Rathore, M. Habes, M. A. Iftikhar, A. Shacklett, C. Davatzikos, A review on neuroimaging-based classification studies and associated feature extraction methods for alzheimer’s disease and its prodromal stages, *NeuroImage* 155 (2017) 530–548.
- [14] K. Fukushima, Neocognitron: A self-organizing neural network model for a mechanism of pattern recognition unaffected by shift in position, *Biological cybernetics* 36 (1980) 193–202.
- [15] Y. LeCun, L. Bottou, Y. Bengio, P. Haffner, Gradient-based learning applied to document recognition, *Proceedings of the IEEE* 86 (1998) 2278–2324.
- [16] A. Yakkundi, Alzheimer’s disease dataset, <https://doi.org/10.17632/ch87yswbz4.1>, 2023. doi:10.17632/ch87yswbz4.1, mendeley Data, Version 1.
- [17] G. Rauterberg, Quantitative test metrics to measure the quality of user interfaces, in: 4th Annual conference software testing analysis and review-EuroSTAR 96, Amsterdam, 2-6 December 1996, EuroSTAR Secretariat, 1996, pp. TQ2P2–1.

A. Online Resources

The MEDIGUI-ConvNet’s code is available via <https://github.com/lucazammataro/MEDIGUI-ConvNet.git> and it is released under GNU General Public License v3.0.